Energy and system-size dependence of two- and four-particle v2 measurements in heavy-ion collisions at √sNN=62.4 and 200 GeV and their implications on flow fluctuations and nonflow

(STAR Collaboration) Agakishiev, G.; ...; Planinić, Mirko; ...; Poljak, Nikola; ...; Zoulkarneeva, Y.

Journal article, Published version
Rad u časopisu, Objavljena verzija rada (izdavačev PDF)

Permanent link / Trajna poveznica: https://urn.nsk.hr/urn:nbn:hr:217:735589

Download date / Datum preuzimanja: **2022-08-24**

Repository / Repozitorij:

Repository of Faculty of Science - University of Zagreb

Energy and system-size dependence of two- and four-particle v_2 measurements in heavy-ion collisions at $\sqrt{s_{NN}} = 62.4$ and 200 GeV and their implications on flow fluctuations and nonflow

G. Agakishiev,[17] M. M. Aggarwal,[29] Z. Ahammed,[47] A. V. Alakhverdyants,[17] I. Alekseev,[15] J. Alford,[18] B. D. Anderson,[18]
C. D. Anson,[27] D. Arkhipkin,[2] G. S. Averichev,[17] J. Balewski,[22] D. R. Beavis,[2] N. K. Behera,[13] R. Bellwied,[43]
M. J. Betancourt,[22] R. R. Betts,[7] A. Bhasin,[16] A. K. Bhati,[29] H. Bichsel,[49] J. Bielcik,[9] J. Bielcikova,[10] L. C. Bland,[2]
I. G. Bordyuzhin,[15] W. Borowski,[40] J. Bouchet,[18] E. Braidot,[26] A. V. Brandin,[25] A. Bridgeman,[1] S. G. Brovko,[4] E. Bruna,[52]
S. Bueltmann,[28] I. Bunzarov,[17] T. P. Burton,[2] X. Z. Cai,[39] H. Caines,[52] M. Calderón de la Barca Sánchez,[4]
D. Cebra,[4] R. Cendejas,[5] M. C. Cervantes,[41] P. Chaloupka,[10] S. Chattopadhyay,[47] H. F. Chen,[37] J. H. Chen,[39] J. Y. Chen,[51]
L. Chen,[51] J. Cheng,[44] M. Cherney,[8] A. Chikanian,[52] K. E. Choi,[33] W. Christie,[2] P. Chung,[10] M. J. M. Codrington,[41]
R. Corliss,[22] J. G. Cramer,[49] H. J. Crawford,[3] X. Cui,[37] A. Davila Leyva,[42] L. C. De Silva,[43] R. R. Debbe,[2] T. G. Dedovich,[17]
J. Deng,[38] A. A. Derevschikov,[31] R. Derradi de Souza,[6] L. Didenko,[2] P. Djawotho,[41] X. Dong,[21] J. L. Drachenberg,[41]
J. E. Draper,[4] C. M. Du,[20] J. C. Dunlop,[2] L. G. Efimov,[17] M. Elnimr,[50] J. Engelage,[3] G. Eppley,[35] M. Estienne,[40] L. Eun,[30]
O. Evdokimov,[7] R. Fatemi,[19] J. Fedorisin,[17] R. G. Fersch,[19] P. Filip,[17] E. Finch,[52] V. Fine,[2] Y. Fisyak,[2] C. A. Gagliardi,[41]
D. R. Gangadharan,[27] F. Geurts,[35] P. Ghosh,[47] Y. N. Gorbunov,[8] A. Gordon,[2] O. G. Grebenyuk,[21] D. Grosnick,[46] D. Gupta,[16]
S. Gupta,[16] W. Guryn,[2] B. Haag,[4] O. Hajkova,[9] A. Hamed,[41] L-X. Han,[39] J. W. Harris,[52] J. P. Hays-Wehle,[22] M. Heinz,[52]
S. Heppelmann,[30] A. Hirsch,[32] G. W. Hoffmann,[42] D. J. Hofman,[7] B. Huang,[37] H. Z. Huang,[5] T. J. Humanic,[27] L. Huo,[41]
G. Igo,[5] W. W. Jacobs,[14] C. Jena,[12] F. Jin,[39] J. Joseph,[18] E. G. Judd,[3] S. Kabana,[40] K. Kang,[44] J. Kapitan,[10] K. Kauder,[7]
H. W. Ke,[51] D. Keane,[18] A. Kechechyan,[17] D. Kettler,[49] D. P. Kikola,[32] J. Kiryluk,[21] A. Kisiel,[48] V. Kizka,[17] S. R. Klein,[21]
A. G. Knospe,[52] D. D. Koetke,[46] T. Kollegger,[11] J. Konzer,[32] I. Koralt,[28] L. Koroleva,[15] W. Korsch,[19] L. Kotchenda,[25]
V. Kouchpil,[10] P. Kravtsov,[25] K. Krueger,[1] M. Krus,[9] L. Kumar,[18] M. A. C. Lamont,[2] J. M. Landgraf,[2] S. LaPointe,[50] J. Lauret,[2]
A. Lebedev,[2] R. Lednicky,[17] J. H. Lee,[2] W. Leight,[22] M. J. LeVine,[2] C. Li,[37] L. Li,[42] N. Li,[51] W. Li,[39] X. Li,[32] X. Li,[38] Y. Li,[44]
Z. M. Li,[51] L. M. Lima,[36] M. A. Lisa,[27] F. Liu,[51] H. Liu,[4] J. Liu,[35] T. Ljubicic,[2] W. J. Llope,[35] R. S. Longacre,[2] Y. Lu,[37]
E. V. Lukashov,[25] X. Luo,[37] G. L. Ma,[39] Y. G. Ma,[39] D. P. Mahapatra,[12] R. Majka,[52] O. I. Mall,[4] R. Manweiler,[46] S. Margetis,[18]
C. Markert,[42] H. Masui,[21] H. S. Matis,[21] D. McDonald,[35] T. S. McShane,[8] A. Meschanin,[31] R. Milner,[22] N. G. Minaev,[31]
S. Mioduszewski,[41] M. K. Mitrovski,[2] Y. Mohammed,[41] B. Mohanty,[47] M. M. Mondal,[47] B. Morozov,[15] D. A. Morozov,[31]
M. G. Munhoz,[36] M. K. Mustafa,[32] M. Naglis,[21] B. K. Nandi,[13] T. K. Nayak,[47] L. V. Nogach,[31] S. B. Nurushev,[31] G. Odyniec,[21]
A. Ogawa,[2] K. Oh,[33] A. Ohlson,[52] V. Okorokov,[25] E. W. Oldag,[42] R. A. N. Oliveira,[36] D. Olson,[21] M. Pachr,[9] B. S. Page,[14]
S. K. Pal,[47] Y. Pandit,[18] Y. Panebratsev,[17] T. Pawlak,[48] H. Pei,[7] T. Peitzmann,[26] C. Perkins,[3] W. Peryt,[48] P. Pile,[2] M. Planinic,[53]
J. Pluta,[48] D. Plyku,[28] N. Poljak,[53] J. Porter,[21] A. M. Poskanzer,[21] C. B. Powell,[21] D. Prindle,[49] C. Pruneau,[50] N. K. Pruthi,[29]
P. R. Pujahari,[13] J. Putschke,[52] H. Qiu,[20] R. Raniwala,[34] S. Raniwala,[34] R. Redwine,[22] R. Reed,[4] H. G. Ritter,[21] J. B. Roberts,[35]
O. V. Rogachevskiy,[17] J. L. Romero,[4] L. Ruan,[2] J. Rusnak,[10] N. R. Sahoo,[47] I. Sakrejda,[21] S. Salur,[4] J. Sandweiss,[52]
E. Sangaline,[4] A. Sarkar,[13] J. Schambach,[42] R. P. Scharenberg,[32] J. Schaub,[46] A. M. Schmah,[21] N. Schmitz,[23] T. R. Schuster,[11]
J. Seele,[22] J. Seger,[8] I. Selyuzhenkov,[14] P. Seyboth,[23] N. Shah,[5] E. Shahaliev,[17] M. Shao,[37] B. Sharma,[29] M. Sharma,[50]
S. S. Shi,[51] Q. Y. Shou,[39] E. P. Sichtermann,[21] F. Simon,[23] R. N. Singaraju,[47] M. J. Skoby,[32] N. Smirnov,[52] D. Solanki,[34]
P. Sorensen,[2] U. G. de Souza,[36] H. M. Spinka,[1] B. Srivastava,[32] T. D. S. Stanislaus,[46] S. G. Steadman,[22] J. R. Stevens,[14]
R. Stock,[11] M. Strikhanov,[25] B. Stringfellow,[32] A. A. P. Suaide,[36] M. C. Suarez,[7] N. L. Subba,[18] M. Sumbera,[10] X. M. Sun,[21]
Y. Sun,[37] Z. Sun,[20] B. Surrow,[22] D. N. Svirida,[15] T. J. M. Symons,[21] A. Szanto de Toledo,[36] J. Takahashi,[6] A. H. Tang,[2]
Z. Tang,[37] L. H. Tarini,[50] T. Tarnowsky,[24] D. Thein,[42] J. H. Thomas,[21] J. Tian,[39] A. R. Timmins,[43] D. Tlusty,[10] M. Tokarev,[17]
S. Trentalange,[5] R. E. Tribble,[41] P. Tribedy,[47] B. A. Trzeciak,[48] O. D. Tsai,[5] T. Ullrich,[2] D. G. Underwood,[1] G. Van Buren,[2]
G. van Nieuwenhuizen,[22] J. A. Vanfossen Jr.,[18] R. Varma,[13] G. M. S. Vasconcelos,[6] A. N. Vasiliev,[31] F. Videbæk,[2]
Y. P. Viyogi,[47] S. Vokal,[17] S. A. Voloshin,[50] M. Wada,[42] M. Walker,[22] F. Wang,[32] G. Wang,[5] H. Wang,[24] J. S. Wang,[20]
Q. Wang,[32] X. L. Wang,[37] Y. Wang,[44] G. Webb,[19] J. C. Webb,[2] G. D. Westfall,[24] C. Whitten Jr.,[5,54] H. Wieman,[21]
S. W. Wissink,[14] R. Witt,[45] W. Witzke,[19] Y. F. Wu,[51] Z. Xiao,[44] W. Xie,[32] H. Xu,[20] N. Xu,[21] Q. H. Xu,[38] W. Xu,[5] Y. Xu,[37]
Z. Xu,[2] L. Xue,[39] Y. Yang,[20] Y. Yang,[51] P. Yepes,[35] K. Yip,[2] I-K. Yoo,[33] M. Zawisza,[48] H. Zbroszczyk,[48] W. Zhan,[20]
J. B. Zhang,[51] S. Zhang,[39] W. M. Zhang,[18] X. P. Zhang,[44] Y. Zhang,[21] Z. P. Zhang,[37] F. Zhao,[5] J. Zhao,[39] C. Zhong,[39] X. Zhu,[44]
Y. H. Zhu,[39] and Y. Zoulkarneeva[17]

(STAR Collaboration)

[1]*Argonne National Laboratory, Argonne, Illinois 60439, USA*
[2]*Brookhaven National Laboratory, Upton, New York 11973, USA*
[3]*University of California, Berkeley, California 94720, USA*
[4]*University of California, Davis, California 95616, USA*
[5]*University of California, Los Angeles, California 90095, USA*
[6]*Universidade Estadual de Campinas, Sao Paulo, Brazil*
[7]*University of Illinois at Chicago, Chicago, Illinois 60607, USA*
[8]*Creighton University, Omaha, Nebraska 68178, USA*
[9]*Czech Technical University in Prague, FNSPE, Prague, 115 19, Czech Republic*
[10]*Nuclear Physics Institute AS CR, 250 68 Řež/Prague, Czech Republic*

[11]*University of Frankfurt, Frankfurt, Germany*
[12]*Institute of Physics, Bhubaneswar 751005, India*
[13]*Indian Institute of Technology, Mumbai, India*
[14]*Indiana University, Bloomington, Indiana 47408, USA*
[15]*Alikhanov Institute for Theoretical and Experimental Physics, Moscow, Russia*
[16]*University of Jammu, Jammu 180001, India*
[17]*Joint Institute for Nuclear Research, Dubna 141 980, Russia*
[18]*Kent State University, Kent, Ohio 44242, USA*
[19]*University of Kentucky, Lexington, Kentucky 40506-0055, USA*
[20]*Institute of Modern Physics, Lanzhou, China*
[21]*Lawrence Berkeley National Laboratory, Berkeley, California 94720, USA*
[22]*Massachusetts Institute of Technology, Cambridge, Massachusetts 02139-4307, USA*
[23]*Max-Planck-Institut für Physik, Munich, Germany*
[24]*Michigan State University, East Lansing, Michigan 48824, USA*
[25]*Moscow Engineering Physics Institute, Moscow Russia*
[26]*NIKHEF and Utrecht University, Amsterdam, The Netherlands*
[27]*Ohio State University, Columbus, Ohio 43210, USA*
[28]*Old Dominion University, Norfolk, Virginia 23529, USA*
[29]*Panjab University, Chandigarh 160014, India*
[30]*Pennsylvania State University, University Park, Pennsylvania 16802, USA*
[31]*Institute of High Energy Physics, Protvino, Russia*
[32]*Purdue University, West Lafayette, Indiana 47907, USA*
[33]*Pusan National University, Pusan, Republic of Korea*
[34]*University of Rajasthan, Jaipur 302004, India*
[35]*Rice University, Houston, Texas 77251, USA*
[36]*Universidade de Sao Paulo, Sao Paulo, Brazil*
[37]*University of Science & Technology of China, Hefei 230026, China*
[38]*Shandong University, Jinan, Shandong 250100, China*
[39]*Shanghai Institute of Applied Physics, Shanghai 201800, China*
[40]*SUBATECH, Nantes, France*
[41]*Texas A&M University, College Station, Texas 77843, USA*
[42]*University of Texas, Austin, Texas 78712, USA*
[43]*University of Houston, Houston, Texas 77204, USA*
[44]*Tsinghua University, Beijing 100084, China*
[45]*United States Naval Academy, Annapolis, Maryland 21402, USA*
[46]*Valparaiso University, Valparaiso, Indiana 46383, USA*
[47]*Variable Energy Cyclotron Centre, Kolkata 700064, India*
[48]*Warsaw University of Technology, Warsaw, Poland*
[49]*University of Washington, Seattle, Washington 98195, USA*
[50]*Wayne State University, Detroit, Michigan 48201, USA*
[51]*Institute of Particle Physics, CCNU (HZNU), Wuhan 430079, China*
[52]*Yale University, New Haven, Connecticut 06520, USA*
[53]*University of Zagreb, Zagreb HR-10002, Croatia*
[54]*Deceased.*

We present STAR measurements of azimuthal anisotropy by means of the two- and four-particle cumulants v_2 ($v_2\{2\}$ and $v_2\{4\}$) for Au + Au and Cu + Cu collisions at center-of-mass energies $\sqrt{s_{NN}} = 62.4$ and 200 GeV. The difference between $v_2\{2\}^2$ and $v_2\{4\}^2$ is related to v_2 fluctuations (σ_{v_2}) and nonflow (δ_2). We present an upper limit to σ_{v_2}/v_2. Following the assumption that eccentricity fluctuations σ_ε dominate v_2 fluctuations $\frac{\sigma_{v_2}}{v_2} \approx \frac{\sigma_\varepsilon}{\varepsilon}$ we deduce the nonflow implied for several models of eccentricity fluctuations that would be required for consistency with $v_2\{2\}$ and $v_2\{4\}$. We also present results on the ratio of v_2 to eccentricity.

I. INTRODUCTION

In noncentral heavy-ion collisions, the overlap area is almond shaped with a long and short axis. Secondary interactions amongst the system's constituents can convert the initial coordinate-space anisotropy to a momentum-space anisotropy in the final state [1–3]. In this case, the *spatial* anisotropy decreases as the system expands so any observed *momentum*

anisotropy will be most sensitive to the early phase of the evolution before the spatial asymmetry is smoothed [4]. Ultra-relativistic nuclear collisions at Brookhaven National Laboratory's Relativistic Heavy Ion Collider (RHIC) [5] are studied in part to deduce whether quarks and gluons become deconfined during the early, high-energy-density phase of these collisions. Since the azimuthal momentum-space anisotropy of particle production is sensitive to the early phase of the collision's evolution, observables measuring this anisotropy are especially interesting. The azimuth angle (ϕ) dependence of the distribution of particle momenta can be expressed in the form of a Fourier series [6], $dN/d\phi \propto 1 + \sum_n 2v_n \cos n(\phi - \Psi)$, where Ψ is either the reaction-plane angle defined by the beam axis and the impact parameter vectors, or the participant plane angle defined by the beam direction and the minor axis of the overlap zone [7]. Fluctuations in the positions of nucleons within the colliding nuclei can cause deviations between the reaction plane angle and the participant plane angle and the nonsphericity of the colliding nuclei may also enhance this effect. When energy is deposited in the overlap region by a finite number of collision participants, the energy density will necessarily possess a lumpiness associated with statistical fluctuations. These fluctuations will lead to eccentricity fluctuations which can contribute to v_2 fluctuations. By definition, the eccentricity is maximum when calculated with respect to the participant plane. This plane shifts away from the reaction plane due to fluctuations. It is expected that this larger, positive definite eccentricity will drive the anisotropic expansion thought to be responsible for v_2 [7]. The eccentricity calculated with respect to the participant axis is called $\varepsilon_{\mathrm{part}}$ and the eccentricity calculated with respect to the reaction plane is called $\varepsilon_{\mathrm{std}}$.

The Fourier coefficients v_n can be measured and used to characterize the azimuthal anisotropy of particle production. Measurements of v_2 [8] have been taken to indicate the matter created in collisions at RHIC behaves like a perfect liquid with a viscosity-to-entropy ratio near a lower bound $\eta/s > 1/4\pi$ derived both from the uncertainty principle [9] and string theory [10]. This conclusion is primarily based on hydrodynamic model predictions [8,11]. Uncertainty about the conditions at the beginning of the hydrodynamic expansion, however, leads to large uncertainties in the model expectations [12,13]. Since v_2 reflects the initial spatial eccentricity of the overlap region when two nuclei collide, fluctuations of v_2 should depend on fluctuations in the initial eccentricity and on how well the expansion phase converts those fluctuations into v_2 fluctuations: Instabilities in an expansion phase may also contribute to v_2 fluctuations. Measurements of the system-size and energy dependence of v_2 and v_2 fluctuations are, therefore, useful for understanding the initial conditions of the expansion phase of heavy-ion collisions and whether low-viscosity hydrodynamic models can accurately predict the behavior of the expansion phase.

Methods used to study v_2 [14] are based on correlations either among produced particles or between produced particles and spectator neutrons detected near beam rapidity y_{beam}. Estimates of v_2 from produced particles can be biased by correlations which are not related to the reaction or participant plane (nonflow $\delta_2 \equiv \langle \cos(2\Delta\phi) \rangle - \langle v_2^2 \rangle$) and by event-by-

event fluctuations of v_2 (σ_{v_2}). Thus, an explicit measurement of $\langle v_2 \rangle$ would require a measurement of nonflow and fluctuations. We also note that when the definition of the reference frame changes, from reaction plane to participant plane, for example, each of the terms v_2, δ_2, and σ_{v_2} can change. The experimentally observable n-particle cumulants of v_2 (labeled $v_2\{2\}^2$, $v_2\{4\}^4$, etc.) do not, however, depend on the choice of reference frame. In addition, the difference between n-particle cumulants provides information about the width and shape of the event-to-event v_2 distribution. The relationship between these cumulants therefore can be compared to cumulants of the initial eccentricity distributions to test how faithfully the v_2 distributions follow the eccentricity distributions.

It has been shown [15–17] that the various analyses of v_2 based on produced particles can be related to the second and fourth v_2 cumulants $v_2\{2\}$ and $v_2\{4\}$ where these are related to v_2, nonflow, and fluctuations in the participant plane reference frame via

$$v_2\{4\}^2 \approx \langle v_2 \rangle^2 - \sigma_{v_2}^2 \qquad (1)$$

and

$$v_2\{2\}^2 - v_2\{4\}^2 \approx \delta_2 + 2\sigma_{v_2}^2. \qquad (2)$$

The approximations are valid for $\sigma_{v_2}/\langle v_2 \rangle \ll 1$ (We discuss the effect of this approximation later.) In case the v_2 distribution is a 2D Gaussian in the reaction plane, the six-particle cumulant $v_2\{6\}$ and higher orders will be equal to $v_2\{4\}$ and therefore will add no new information. This has been found to be the case (i.e., $v_2\{6\} \approx v_2\{4\}$) to within 3% for previous data sets [18] and to within less than 2% for the Au + Au data sets used in this analysis. In this approximation for the v_2 fluctuations [17], $v_2\{4\}$ is equal to the mean v_2 relative to the reaction plane and $\sqrt{v_2^2\{4\} + \sigma_{v_2}^2}$ is the mean v_2 relative to the participant plane. We note again that $\sigma_{v_2}^2$ is not experimentally accessible without prior knowledge about nonflow contributions [19].

In this paper we present measurements of $v_2\{2\}$ and $v_2\{4\}$ in Au + Au and Cu + Cu collisions at $\sqrt{s_{NN}} = 200$ and 62.4 GeV. We present $v_2\{2\}^2 - v_2\{4\}^2 \approx \delta_2 + 2\sigma_{v_2}^2$ (called in the literature σ_{tot}^2) and derive from that upper limits on σ_{v_2}/v_2 based on several approximations. The upper limit assumes that v_2 fluctuations dominate the sum $\delta_2 + 2\sigma_{v_2}^2$. This is a robust upper limit since larger values of σ_{v_2}/v_2 would require negative values of nonflow contrary to expectations and to measurements of two-particle correlations [20]. We present model comparisons of eccentricity fluctuations to the upper limit of σ_{v_2}/v_2. Alternatively, using the same data and assuming that eccentricity fluctuations drive v_2 fluctuations, we can derive the nonflow term required to satisfy the relationship $v_2\{2\}^2 - v_2\{4\}^2 \approx \delta_2 + 2\sigma_{v_2}^2$ for each model. The δ_2 derived in this way can be compared to measurements of two-particle correlations [20] to check the validity of the models. Finally, we present the ratio of v_2 to the initial eccentricity from the models. Our comparisons allow us to assess how well the proportionality between v_2 and eccentricity holds both on an event-by-event basis and across system-size and colliding energy. Both of these are useful for understanding the nature of the matter created in heavy-ion collisions.

In this paper, we do not make use of a two-dimensional fit to an 11-parameter model of two-particle correlations in relative pseudorapidity and azimuth as in Ref. [21]. We, instead, forego any assumptions about the shape of flow fluctuations or nonflow and consider only Fourier harmonics of the azimuthal distributions integrated over the midrapidity region of the STAR detector.

This paper is organized as follows: Section II gives the experimental details and cuts for the data selection. Section III deals with details about the Q-cumulants method and the sources of systematic errors. In Sec. IV, v_2 results used in the calculation of the nonflow and the upper limit on v_2 fluctuations are discussed. Section V shows the results for the upper limit on v_2 fluctuations and their comparison with the eccentricity fluctuations, nonflow from different models, and eccentricity scaling of v_2 for the eccentricity from different models.

II. EXPERIMENT

Our data sets were collected from Au + Au and Cu + Cu collisions at $\sqrt{s_{NN}} = 62.4$ and 200 GeV detected with the STAR detector [22] in runs IV (2004) and V (2005). Charged-particle tracking within pseudorapidity $|\eta| < 1$ and transverse momentum $p_T > 0.15$ GeV/c was performed with the Time Projection Chamber (TPC) [23]. Beam-beam counters (BBCs) and zero-degree calorimeters (ZDCs) were used to trigger on events. We analyzed events from centrality interval corresponding to 0–80% and 0–60% of the hadronic interaction cross-section, respectively, for Au + Au and Cu + Cu collisions. As in previous STAR analyses [24], we define the centrality of an event from the number of charged tracks in the TPC having pseudorapidity $|\eta| < 0.5$ [25]. For the v_2 analysis we used charged tracks with $|\eta| < 1.0$ and $0.15 < p_T < 2.0$ GeV/c. The lower p_T cut is necessitated by the acceptance of the STAR detector. We varied the upper p_T cut between 1.5 and 3.0 GeV/c to study the effect of this cut on the difference $v_2\{2\}^2 - v_2\{4\}^2$. We found that $v_2\{2\}$ and $v_2\{4\}$ increase by roughly 5% (relative) when the upper p_T cut is increased from 1.5 to 3.0 GeV/c but that the difference between $v_2\{2\}^2$ and $v_2\{4\}^2$ changes by less than 1%. Only events with primary vertices within 30 cm of the TPC center in the beam direction were analyzed. The cuts used in the analysis are shown in Table I.

TABLE I. Cuts used for the selection of data. Fit points are the number of points used to fit the TPC track, and max. points are the maximum possible number for that track.

Cut	Value
p_T	0.15 to 2.0 GeV/c
η	−1.0 to 1.0
Vertex z	−30.0 to 30.0 cm
Vertex x, y	−1.0 to 1.0 cm
Fit points	>15
Fit points/max. pts.	>0.52
dca	<3.0 cm
Trigger	Minbias

III. ANALYSIS

We analyzed Cu + Cu and Au + Au collisions at center-of-mass energies $\sqrt{s_{NN}} = 62.4$ and 200 GeV to study the energy and system-size dependence of v_2, nonflow, and v_2 fluctuations. From previous studies we found that it is not possible to use v_2 cumulants to disentangle nonflow effects (correlations not related to the event plane) from v_2 fluctuations [19]. We have used two methods based on multiparticle azimuthal correlations: (i) Q cumulants [26] for two- and four-particle cumulants to study $v_2\{2\}$ and $v_2\{4\}$ (ii) and fitting the reduced flow vector $q = Q/\sqrt{M}$ distribution to study the multiparticle v_2. $Q = \sum_j^M e^{2i\phi_j}$ and M is the multiplicity. The fitting of the reduced flow vector distribution is described in more detail in Ref. [19]. The fit parameters described in that reference, $v_2\{\text{qfit}\}$ and σ_{dyn}^2 (in this paper σ_{tot}^2), can be related to $v_2\{2\}$ and $v_2\{4\}$. In Appendix A, we compare the q-distribution and Q-cumulants results. Based on simulations, we find that the q-distribution method used to study v_2 by fitting the distribution of the magnitude of the reduced flow vector to a function derived from the central limit theorem deviates more from the input values when multiplicity is low. For that reason, this paper presents only results from the Q-cumulants method.

The Q-cumulants method allows us to calculate the cumulants without nested loops over tracks or using generating functions [18]. For this reason it is simpler to perform. The cumulants calculated in this way also do not suffer from interference between different harmonics since the contributions from other harmonics are explicitly removed [26]. We directly calculate the two- and four-particle azimuthal correlations

$$\langle 2 \rangle_{n|n} = \frac{|Q_n|^2 - M}{M(M-1)} \tag{3}$$

$$\langle 4 \rangle_{n,n|n,n} = \frac{|Q_n|^4 + |Q_{2n}|^2 - 2\text{Re}[Q_{2n}Q_n^*Q_n^*]}{M(M-1)(M-2)(M-3)}$$
$$- 2\frac{2(M-2)|Q_n|^2 - M(M-3)}{M(M-1)(M-2)(M-3)}, \tag{4}$$

where M is the number of tracks used in the analysis and

$$Q_n = \sum_j^M e^{in\phi_j}. \tag{5}$$

We evaluate the terms on the right-hand side of Eq. (3) and Eq. (4) for each event, then take the average over all events. If one applies no further weighting, the two- and four-particle cumulant results for v_n are

$$v_n\{2\}^2 = \langle 2 \rangle_{n|n}, \tag{6}$$

$$v_n\{4\}^4 = 2\langle 2 \rangle_{n|n}^2 - \langle 4 \rangle_{n,n|n,n}. \tag{7}$$

It was also proposed to use weights for each event within a particular centrality class based on the number of combinations of tracks for each event [26]. This weighting was proposed as a method to reduce the dependence of the results on multiplicity. We find, however, that the application of number-of-combinations weights makes the $v_2\{2\}$ and $v_2\{4\}$ results more dependent on the width of the multiplicity bins used to define centrality in our analysis. Using number-of-combination weights along with centrality bins defined by number of
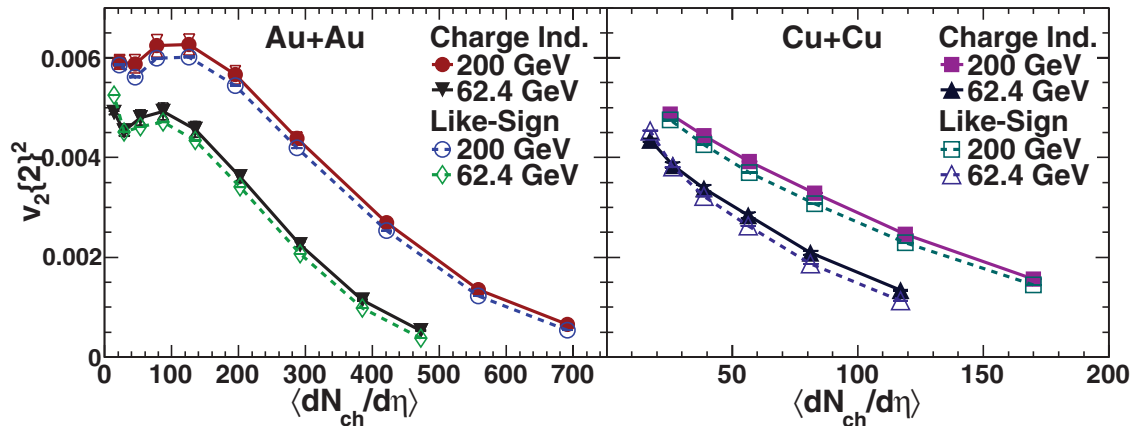
FIG. 1. (Color online) (Left) The two-particle cumulant $v_2\{2\}^2$ for Au + Au collisions at 200 and 62.4 GeV. Results are shown with like-sign combinations (LS) and charge-independent results (CI) for $0.15 < p_T < 2.0$ GeV/c. (Right) The same as the left but for Cu + Cu collisions. The systematic errors are shown as triangles above and below the data points and statistical errors are shown as thick lines with caps at the end. Statistical and systematic errors are very small.

charged particles will lead to results that are weighted more heavily toward the higher multiplicity side of the bins and that effect will be stronger for four-particle correlations than for two-particle correlations. We also confirmed with simulations that without weights, the Q-cumulant results for $v_2\{2\}$ and $v_2\{4\}$ agree better with simulation inputs than when weights are applied. In this paper, we report results without weights according to Eqs. (3) through (7). This method differs from that used in Ref. [27].

The systematic uncertainties on our measurements were estimated by evaluating our results from two different time periods in the run, by varying the selection criteria on the tracks (specifically the distance of closest approach of the track to the primary vertex or DCA where tighter DCA cuts should reduce the number of background tracks), from the Q-cumulants acceptance correction terms, and by varying the p_T upper limit for tracks between 1.5, 2.0, and 3.0 GeV/c. In addition to improving track quality, decreasing the DCA cut also increases the average p_T of the track sample, as does increasing the upper p_T cut of the analyzed tracks. This leads to an increase in $v_2\{2\}$ and $v_2\{4\}$ (not considered a systematic error for those data) but we find that the difference between $v_2\{2\}^2$ and $v_2\{4\}^2$ is nearly unchanged. This implies that the error on $v_2\{2\}^2 - v_2\{4\}^2$ due to the exact upper and lower p_T ranges used is small. We found no difference between the two run periods analyzed. The acceptance correction applied in the analysis changes the 200 GeV Au + Au Q-cumulants $v_2\{4\}$ results by less than 1% for all centralities while the $v_2\{2\}$ results change by less than 1% for all centralities except the 0–5% bin, where they change by 4%, and the 5–10% bin, where they change by 2%. Statistical and systematic errors are shown on all results. The systematic errors are shown as triangles above and below the data points and statistical errors are shown as thick lines with caps. In many cases, statistical errors are smaller than the marker size and, therefore, not visible.

IV. RESULTS

In this paper we present our results as a function of the average charged-particle multiplicity density $\langle dN_{\rm ch}/d\eta \rangle$ within a given centrality interval. Table III in Appendix B provides estimates of the number of participating nucleons $N_{\rm part}$ and $\langle dN_{\rm ch}/d\eta \rangle$ for the centrality intervals used in this analysis. Figure 1 (left) shows $v_2\{2\}^2$ for 200 and 62.4 GeV Au + Au collisions for charged tracks with $0.15 < p_T < 2.0$ GeV/c. The analysis is carried out using either all combinations of particles, independent of charge (CI), or using only like-sign pairs (LS). When comparing the LS and CI results, we note that the LS results are systematically lower than the CI results for all centralities except the most peripheral bin. This behavior might be related to nonflow since many known nonflow effects lead to correlations preferentially between opposite sign particles; e.g., neutral resonances decay into opposite sign particles and jet fragments tend to be charge ordered [28]. The LS results, therefore, typically contain smaller nonflow correlations. Bose-Einstein correlations between identical particles, on the other hand, can lead to larger nonflow for LS than for CI since LS contains a larger sample of identical particles. Figure 1 (right) shows the CI and LS results for Cu + Cu collisions at $\sqrt{s_{NN}} = 200$ and 62.4 GeV. The same trends hold with the LS results lower than the CI results.

Figure 2 shows the difference of CI $v_2\{2\}$ and LS $v_2\{2\}$ for Au + Au and Cu + Cu collisions at 200 and 62.4 GeV. For the lowest multiplicities, CI $v_2\{2\}$ becomes smaller than LS $v_2\{2\}$, consistent with expectations from Bose-Einstein correlations. For other multiplicities, CI $v_2\{2\}$ is systematically larger than LS $v_2\{2\}$. The dominant systematic errors in this comparison come from a variation of the results when the cut on track DCA is varied.

Figure 3 shows the four-particle cumulant $v_2\{4\}^4$ for Au + Au (left) and Cu + Cu (right) collisions at 200 and 62.4 GeV. In the case of $v_2\{4\}^4$, no differences are detected between LS and CI results (see Fig. 4). This suggests that
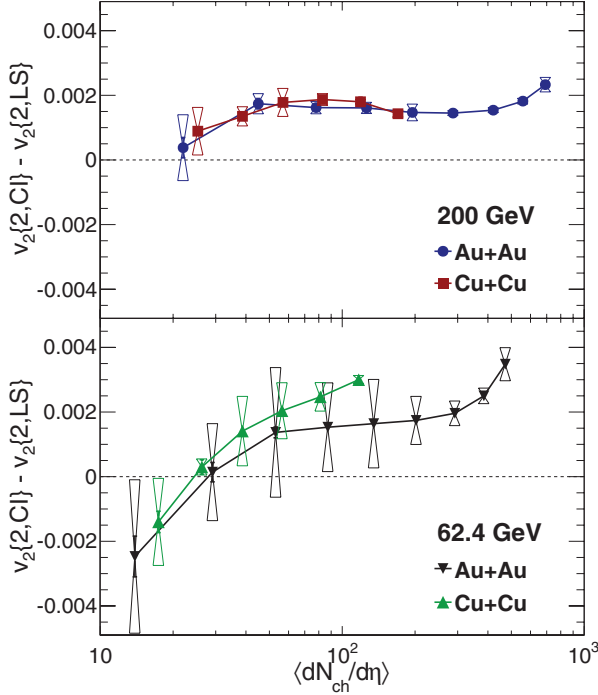
FIG. 2. (Color online) The difference of charge-independent (CI) $v_2\{2\}$ and like-sign (LS) $v_2\{2\}$ for Au + Au and Cu + Cu collisions at 200 (top panel) and 62.4 (bottom panel) GeV vs. the log of $\langle dN_{ch}/d\eta\rangle$. The statistical errors are smaller than the marker size and not visible for most of the data.
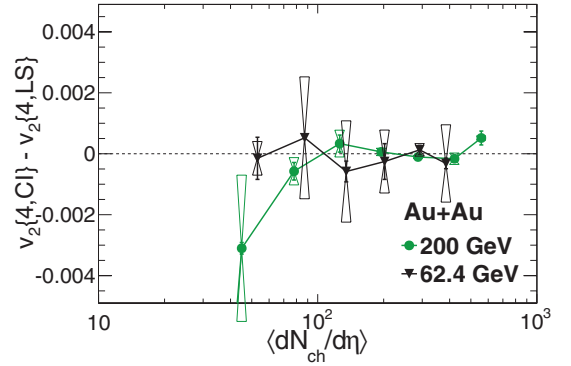

FIG. 4. (Color online) The difference of charge-independent (CI) $v_2\{4\}$ and like-sign (LS) $v_2\{4\}$ for Au + Au collisions at 200 and 62.4 GeV vs. the log of $\langle dN_{ch}/d\eta\rangle$.

nonflow correlations are suppressed as expected in the four-particle cumulant results. Any nonflow source leading to fewer than four correlated particles will not contribute to $v_2\{4\}^4$. In addition, while any nonflow for $v_2\{2\}^2$ is suppressed only by $1/M$, any nonflow correlations between four or more particles will still be suppressed by a combinatorial factor of $(M-1)(M-2)(M-3)$. $v_2\{4\}^4$ shows slightly negative

values for the more central events for Au + Au and Cu + Cu collisions at 200 and 62.4 GeV. $v_2\{4\}^4$ is allowed to take on negative values. These may be associated with v_2 fluctuations larger than those expected from eccentricity fluctuations alone. In this case, however, the second or fourth roots of $v_2\{4\}^4$ cannot be defined. For this reason, those points are not included in the analysis of $v_2\{2\}^2 - v_2\{4\}^2$. All results are reported in the data tables [29]. It had been observed from simulations that the measurement of $v_2\{4\}$ using the Q-cumulants method deviates from input for the most peripheral collisions. Also, the LS $v_2\{4\}$ data appears to scatter for mean charged-particle multiplicity density $\langle dN_{ch}/d\eta\rangle < 26$. Therefore, no data points are used for comparison with models for $\langle dN_{ch}/d\eta\rangle < 26$.

Figure 5 shows $v_2\{2\}^2 - v_2\{4\}^2$ for Au + Au and Cu + Cu collisions at 200 GeV (left) and 62.4 GeV (right) for both LS and CI. The difference between $v_2\{2\}^2$ and $v_2\{4\}^2$ is of interest because it is related to nonflow δ_2 and v_2 fluctuations:

$$v_2\{2\}^2 - v_2\{4\}^2 \approx \delta_2 + 2\sigma_{v_2}^2 \equiv \sigma_{tot}^2. \qquad (8)$$

FIG. 3. (Color online) (Left) The LS and CI four-particle cumulant $v_2\{4\}^4$ for Au + Au collisions at 200 and 62.4 GeV for $0.15 < p_T < 2.0$ GeV/c. The systematic errors are shown as triangles above and below the data points and statistical errors are shown as thick lines with caps at the end. Statistical errors are not visible for most of the points. (Right) The LS and CI four-particle cumulant $v_2\{4\}^4$ for Cu + Cu collisions at 200 and 62.4 GeV for $0.15 < p_T < 2.0$ GeV/c. The most central points (two points for Cu + Cu 62.4 GeV) gives $v_2\{4\}^4 < 0$ for all the data sets. The negative values are probably due to large fluctuations in agreement with Eq. (1). These may include contributions from impact parameter spread and finite multiplicity bin width.
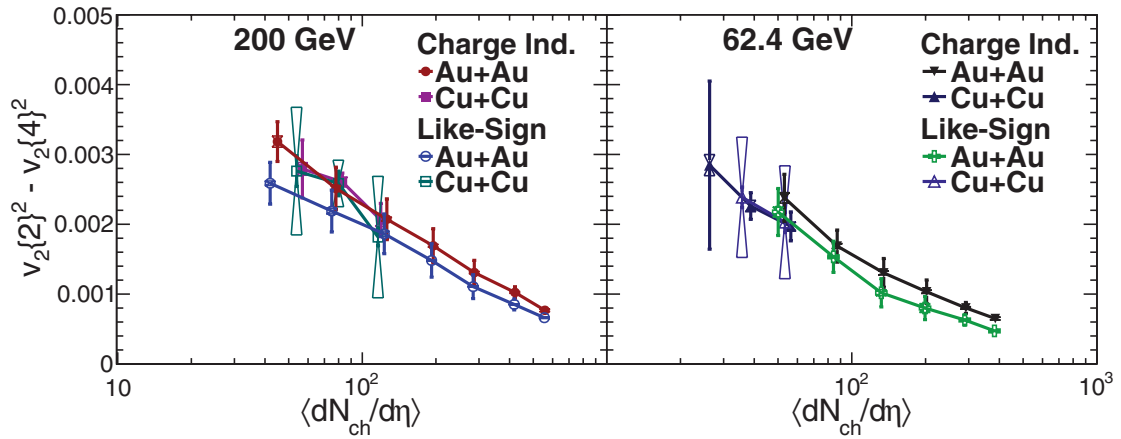
FIG. 5. (Color online) (Left) The difference between $v_2\{2\}^2$ and $v_2\{4\}^2$ for 200 GeV Au + Au and Cu + Cu collisions for both LS and CI combinations. (Right) The difference between $v_2\{2\}^2$ and $v_2\{4\}^2$ for 62.4 GeV Au + Au and Cu + Cu collisions for both LS and CI combinations. The statistical and systematic errors are shown as in previous figures.

This difference can be taken as an approximate upper limit on nonflow δ_2. We estimate that the approximation in Eq. (8) which assumes $\langle v_2 \rangle$ is much larger than the second, third, and fourth moments of v_2 is accurate to within 30% for these data sets. We arrive at this estimate by assuming $v_2 \propto \varepsilon_{\text{part}}$ and then using our Monte Carlo Glauber model to calculate $(\varepsilon_{\text{part}}\{2\}^2 - \varepsilon_{\text{part}}\{4\}^2)/2\sigma^2_{\varepsilon_{\text{part}}}$ ($\varepsilon_{\text{part}}$ calculations are described in Appendix B). If the approximation in Eq. (8) is accurate, this ratio should be unity. We find that for the centralities considered here, the ratio is within 30% of unity (not shown). Below, where we compare our data to eccentricity models, a significant fraction should cancel since the approximation applies to both the data and the models. The difference $v_2\{2\}^2 - v_2\{4\}^2$ increases with beam energy and decreases with increasing mean multiplicity. Due to combinatorics, the contribution from nonflow will scale as $1/\langle dN_{\text{ch}}/d\eta \rangle$ if the number of clusters scales with $\langle dN_{\text{ch}}/d\eta \rangle$ and the number of particles per cluster is constant. Based on the central limit theorem, a $1/N_{\text{part}}$ dependence is also expected for $\sigma^2_{v_2}$ from eccentricity fluctuations (the calculation of eccentricity can be viewed as a nearly random walk with N_{part} steps). The energy dependence can come from either an increase in nonflow correlations with energy and/or an increase in v_2 fluctuations with energy. The LS results are systematically lower than the CI results for all but the lowest multiplicities, consistent with a nonflow contribution to the CI $v_2\{2\}$ results which is reduced for the LS $v_2\{2\}$ results. In the model comparisons that follow, we will use the LS results to compare our results to three eccentricity models.

V. DATA AND ECCENTRICITY MODELS

We compare our $v_2\{2\}$ and $v_2\{4\}$ results characterizing the distribution of v_2, to equivalent measures characterizing the eccentricity distributions of three models. These comparisons may be useful for determining properties of the fireball created in the collisions since the width of the distribution of v_2 is expected to depend on transport properties like viscosity [30].

The models are a Monte Carlo Glauber model with nucleons as participants (MCG-N), a Monte Carlo Glauber model with quarks as participants (MCG-Q), and a CGC based Monte Carlo model (fKLN-CGC). The fKLN-CGC model generates larger eccentricity values while the MCG-N model generates larger fluctuations. The MCG-Q model is found to generally give results intermediate between the two. The models are described in more detail in Appendix B. Another analysis of models has been published in Ref. [31]. The nonsphericity of the Au nuclei has been neglected in eccentricity calculations for the models because nonsphericity only affects the most central collisions which are not used in the comparison of data with models [32].

A. Upper limit on relative fluctuations

We would like to compare our data to models for eccentricity fluctuations by comparing σ_{v_2}/v_2 to $\sigma_\varepsilon/\varepsilon$. We cannot uniquely determine the value of σ_{v_2} from the two- and four-particle cumulant data, however, since $v_2\{2\}^2 - v_2\{4\}^2 \approx \delta_2 + 2\sigma^2_{v_2}$. We can, however, derive an upper limit on the ratio σ_{v_2}/v_2 by setting $\delta_2 = 0$. This amounts to assuming the difference between the two- and four-particle cumulant is dominated by v_2 fluctuations and that δ_2 cannot be negative. Although negative nonflow values can easily be generated from resonance decays in specific kinematic regions, we consider the case that the total nonflow should become negative highly unlikely and contradictory to studies of the nonflow effect. The quantity

$$R_{v(2-4)} = \sqrt{\frac{v_2\{2\}^2 - v_2\{4\}^2}{v_2\{2\}^2 + v_2\{4\}^2}} \tag{9}$$

then becomes an upper limit to the ratio $\sigma_{v_2}/\langle v_2 \rangle$ where, in the case that v_2 fluctuations are dominated by eccentricity fluctuations, $\langle v_2 \rangle$ is the average v_2 relative to the participant axis [17]. Additional fluctuations from another source will lead to a contribution to the difference between $v_2\{2\}$ and $v_2\{4\}$ not related to the eccentricity fluctuations that relate the reaction
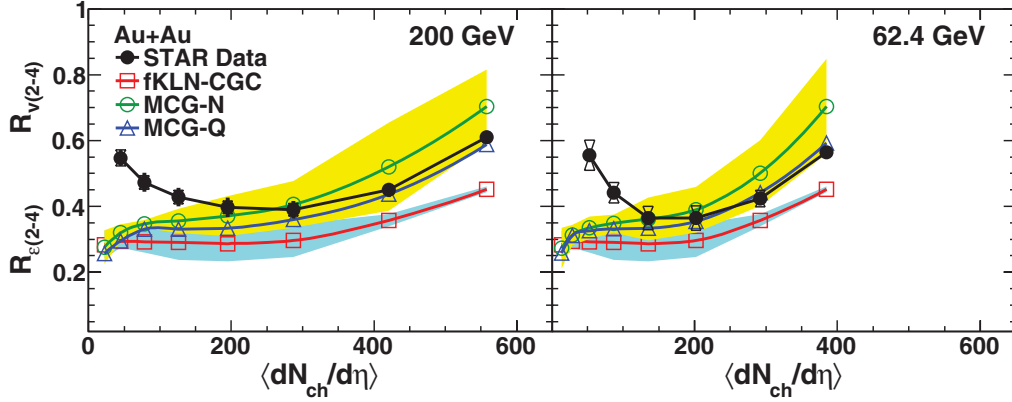
FIG. 6. (Color online) The upper limit on $\sigma_{v_2}/\langle v_2 \rangle$ for 200 GeV (left) and 62.4 GeV (right) Au + Au collisions from Eq. (9) compared to $\sigma_\varepsilon/\varepsilon$ from Eq. (10) for three different models. The upper limit is found using the LS results for $v_2\{2\}$. Data are from the range $0.15 < p_T < 2.0$ GeV/c. The shaded bands reflect the uncertainties on the models which are dominated by uncertainty on the distribution of nucleons inside the nucleus. The uncertainty is only shown for the MCG-N and fKLN-CGC models. The uncertainty on the MCG-Q model is the same as for the MCG-N model but is not shown for the visual clarity.

plane and the participant plane. In the following figures, we compare the ratio $R_{v(2-4)}$ for the like-sign results to the ratio

$$R_{\varepsilon(2-4)} = \sqrt{\frac{\varepsilon\{2\}^2 - \varepsilon\{4\}^2}{\varepsilon\{2\}^2 + \varepsilon\{4\}^2}} \qquad (10)$$

for the three eccentricity models described in Appendix B, where $\varepsilon\{2\}$ and $\varepsilon\{4\}$ are the second and fourth cumulants for $\varepsilon_{\text{part}}$. Since higher moments (skewness and kurtosis) of the distribution of v_2 or ε_2 contribute to Eqs. (9) and (10), it is important to compare the same quantities from data and the eccentricity models. For $\sigma_\varepsilon \ll \varepsilon$ Eq. (10) becomes $\sigma_\varepsilon/\langle\varepsilon\rangle$. We find in our models for eccentricity $R_{\varepsilon(2-4)}$ is within 15% of $\sigma_\varepsilon/\langle\varepsilon\rangle$ for all centralities except the most central where it is 25% larger. If nonflow contributions to $R_{v(2-4)}$ are negligable and $v_2 \propto \varepsilon_2$, then $R_{v(2-4)}$ should coincide with $R_{\varepsilon(2-4)}$.

Figure 6 shows $R_{v(2-4)}$ versus mean charged hadron multiplicity for 200 GeV (left) and 62.4 GeV (right) Au + Au data. The LS $v_2\{2\}$ results are used to reduce nonflow. The data are compared to the same quantity for the three different models. The shaded bands show the uncertainties on the models that arise primarily from the uncertainty in the Woods-Saxon parameters used to describe the nuclei. The error is correlated between Monte Carlo models and for clarity is only plotted on the MCG-Q and fKLN-CGC models. The centrality in the models is defined using multiplicity so the model calculations include bin-width effects and impact parameter fluctuations similar to data. Inasmuch as the models correctly model the multiplicity, by defining centrality in the models the same way that it is defined in data, both the model and the data will have the same impact parameter fluctuations.

In peripheral collisions ($\langle dN_{\text{ch}}/d\eta \rangle < 150$), data exceeds the eccentricity models substantially. This is not surprising since we expect a significant contribution from nonflow in this region. The central value for the ratio from the MCG-N model rises with increasing centrality and then overshoots the upper limit in the most central collisions. Given the errors indicated by the yellow band, however, the MCG-N model could still be

consistent with the upper limit. The MCG-Q model approaches the upper limit in central collisions but never exceeds it. The fKLN-CGC model has the smallest values and is well below the upper limit throughout the entire centrality range. Notice that, in the models, the more constituents, the smaller the fluctuations.

In Fig. 6 (right), the 62.4 GeV Au + Au data are compared to models. Data points are reported only where $v_2\{4\}^4$ is positive. At this lower energy, peripheral data is again above the models. The central value for the MCG-N model again overshoots the upper limit for central and midcentral collisions while the MCG-Q model appears to just reach the upper limit for the most central data point. The uncertainty on the geometry of the Au nucleus again, however, makes it impossible to rule out any of the models in this comparison. The fKLN-CGC model lies below the upper limit for the entire range. The fact that the MCG-N and MCG-Q models reach and in some cases exceed the upper limit means that for those models to be correct, nonflow would have to be small or perhaps even negative. Nonflow can be negative from resonance decay but is not likely. The lower energy data therefore provide a very useful test of the models and results from the beam energy scan at RHIC promise to provide even better constraints [33].

Figure 7 shows the STAR 200 GeV Au + Au data on the upper limit for $\sigma_{v_2}/\langle v_2 \rangle$ compared to the PHOBOS results reported in Ref. [34] under their assumption that δ_2 is zero for $\Delta\eta > 2$ (see the reference for details). The PHOBOS results are for all charged particles while the STAR results are for LS pairs only. PHOBOS has subtracted narrow $\Delta\eta$ correlations by fitting $v_2(\eta_1)v_2(\eta_2)$ and removing the narrow diagonal peak corresponding to small-$\Delta\eta$ nonflow correlations. This may explain why the PHOBOS results are slightly below the STAR upper limits derived from LS $v_2\{2\}$, suggesting that there may be some residual nonflow in our LS results. We also note, however, that the analysis procedures in this paper and in the PHOBOS paper differ substantially.

Figure 8 shows the upper limits and models for Cu + Cu collisions at 200 and 62.4 GeV (respectively left and right).
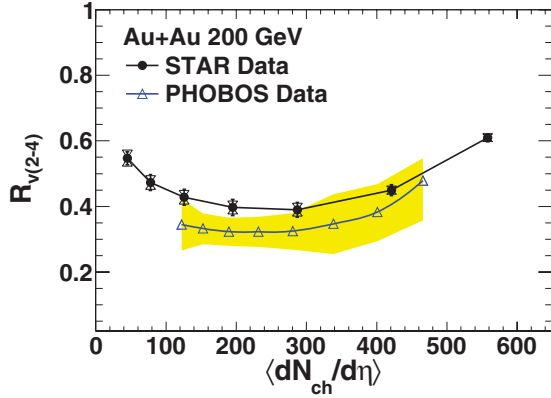
FIG. 7. (Color online) The STAR data compared to PHOBOS data [34] on $\sigma_{v_2}/\langle v_2 \rangle$ with δ_2 for $\Delta\eta > 2$ taken to be zero (see Fig. 6 from Ref. [34]). The shaded band shows the errors quoted from Ref. [34].

Data points are only reported where $v_2\{4\}^4$ is positive. The upper limit on fluctuations for Cu + Cu collisions are larger than for Au + Au and lie near unity. All the models fall below the upper limit and differences between the models are small. This is likely due to the large multiplicity fluctuations for smaller systems in the models which masks the other physical differences between the models. The large Cu + Cu results do not provide constraint on the models. Once the systematic errors on the models are taken into account, all the models are within the upper limits on v_2 fluctuations imposed by $v_2\{2\}$ and $v_2\{4\}$.

B. Nonflow

Eccentricity fluctuations are just one of the mechanisms that could contribute to the difference between $v_2\{2\}^2$ and $v_2\{4\}^2$. In addition to fluctuations from an expansion phase (induced by viscous effects for example), nonflow correlations are thought to contribute substantially. In order to assess the contribution of nonflow to the to the difference between $v_2\{2\}^2$ and $v_2\{4\}^2$ we estimate the contribution to v_2 fluctuations from

from eccentricity fluctuations by taking

$$\sigma_{v_2} \approx \langle v_2 \rangle \frac{\sigma_\varepsilon}{\varepsilon} \qquad (11)$$

and then derive the width impled by each eccentricity model. We will make the assumption that other sources to v_2 fluctuations are small so the residual is dominated by nonflow δ_2. Note that, in Eq. (11), $\langle v_2 \rangle$ is not directly observable. Following this assumption, we can calculate the value of δ_2 that would be needed to satisfy the following equation:

$$v_2\{2\}^2 - v_2\{4\}^2 \approx \delta_2 + 2\sigma_{v_2}^2. \qquad (12)$$

Recalling from Eqs. (1) and (2) that $v_2\{2\}^2 + v_2\{4\}^2 \approx \delta_2 + 2\langle v_2 \rangle^2$, we derive the following expression for δ_2:

$$\delta_2 \approx v_2\{2\}^2 - v_2\{4\}^2 \left(\frac{\varepsilon^2 + \sigma_\varepsilon^2}{\varepsilon^2 - \sigma_\varepsilon^2} \right). \qquad (13)$$

which depends only on the directly observable cumulants and quantities obtained from models. Since a model dependence exists, the δ_2 values are not measurements of δ_2 but instead provide an alternative consistency check for the models. These values can be compared to other measurements of nonflow correlations such as the already measured two-particle correlations [21]. This is an important test for the models, since a complete model of heavy-ion collisions should be able to predict multiple observables at once. The interpretation, however, of the structures in two-particle correlations such as the ridge [21] is in flux. In particular, the nonflow correlations from jets are inferred from two-particle correlations versus $\Delta\eta$ and $\Delta\phi$ after subtracting a $\Delta\eta$ independent v_2^2 term. This approximation may not be valid for reasons discussed recently in the literature [35]. Given the current state of understanding, in this paper we do not make a direct comparison of the nonflow correlations inferred from this analysis to those inferred from two-particle correlations.

In the absence of new physics, the term δ_2 will vary with event multiplicity as $1/M$. This is because, in the case that high multiplicity events are a linear superposition of lower-multiplicity events, the numerator in the mean grows as M while the denominator grows as the number of pairs $M(M - 1)/2$. To cancel out the combinatorial $1/M$ dependence we
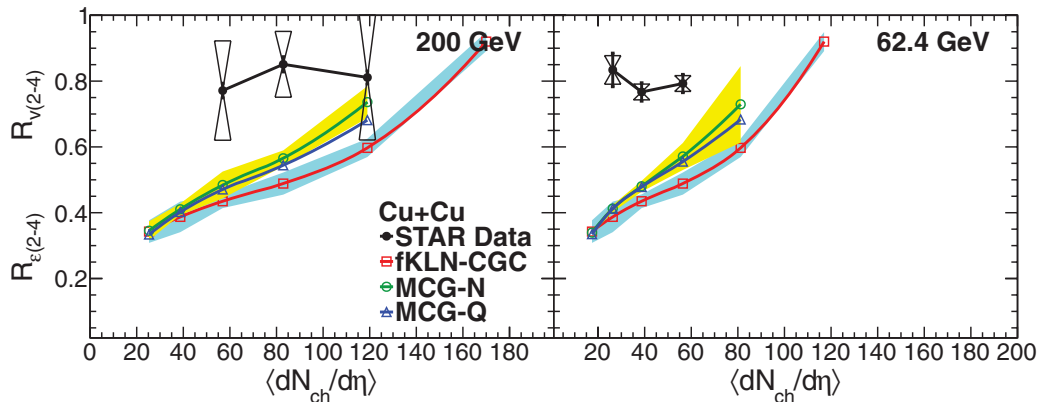

FIG. 8. (Color online) The upper limit on $\sigma_{v_2}/\langle v_2 \rangle$ for 200 GeV (left) and 62.4 GeV (right) Cu + Cu collisions from Eq. (9) compared to $\sigma_\varepsilon/\varepsilon$ from Eq. (10) for three different models.
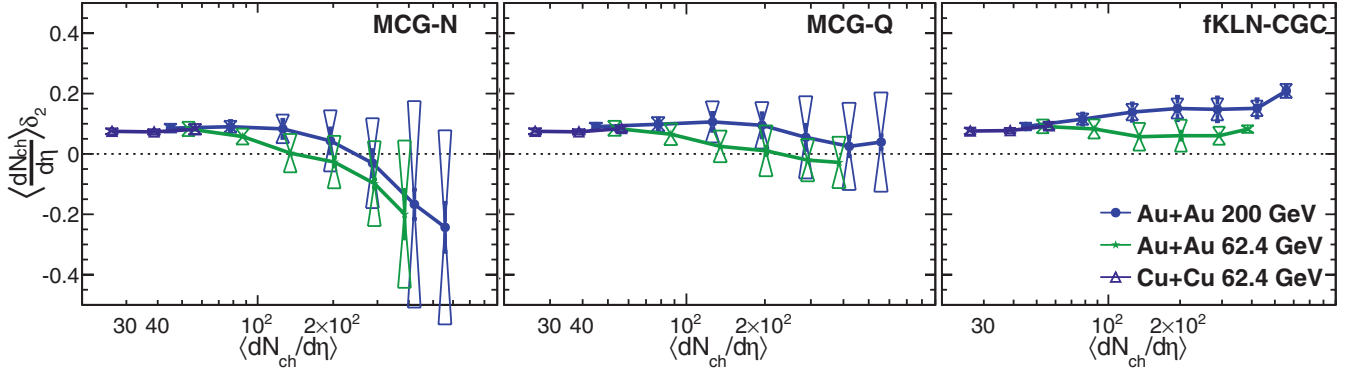
FIG. 9. (Color online) The mean multiplicity scaled nonflow (δ_2) found by assuming Eq. (11) and using the three different models for $\sigma_\varepsilon^2/\varepsilon^2$: MCG-N (left), MCG-Q (middle), and fKLN-CGC (right). The systematic errors are shown as triangles above and below the data points and statistical errors are shown as thick lines with caps. Statistical errors are not visible for most of the points. For clarity, the 200-GeV Cu + Cu data with large point-to-point systematic errors are excluded. For the other data sets the systematic errors are highly correlated but centrality dependent.

scale δ_2 by the number of mean charged hadrons within $|\eta| < 0.5$. A variation of $\langle \frac{dN_{ch}}{d\eta} \rangle \delta_2$ with multiplicity implies a nontrivial change in the physics.

Figure 9 (left) shows the like-sign $\langle \frac{dN_{ch}}{d\eta} \rangle \delta_2$ that is required if the Monte Carlo Glauber model with nucleon participants gives the correct description of the eccentricity fluctuations and eccentricity fluctuations dominate v_2 fluctuations. The nonflow is larger at 200 GeV than at 62.4 GeV. Within errors, $\langle \frac{dN_{ch}}{d\eta} \rangle \delta_2$ is the same in Cu + Cu collisions and Au + Au collisions at the same energies and event multiplicities. The errors shown in the figure are dominated by the systematic errors on the MCG-N model arising from the uncertainty in the Woods-Saxon parameters which are highly correlated from point to point but are also centrality dependent (they cannot be described as a single centrality-independent shift). The most central data point is only consistent with zero for a very limited range for the Woods-Saxon parameters describing the charge distribution in the nucleus. For this model of eccentricity fluctuations to be valid, the nonflow in central Au + Au collisions would have to be near zero or negative. If the near-side two-particle correlations [21,36] observed in data are due to nonflow, then they would directly contradict the MCG-N description of eccentricity. In the case that there is a dynamical component to the v_2 fluctuations related to dissipative effects [30], the inferred nonflow would need to become even smaller or more negative.

Figure 9 (middle) shows the $\langle \frac{dN_{ch}}{d\eta} \rangle \delta_2$ required if the Monte Carlo Glauber model with constituent quark participants gives the correct description of the eccentricity fluctuations and if eccentricity fluctuations dominate v_2 fluctuations. Within errors, $\langle \frac{dN_{ch}}{d\eta} \rangle \delta_2$ is the same in Cu + Cu collisions and Au + Au collisions at the same energies and event multiplicities. The smaller relative fluctuations for the constituent quark participant model means this model would be consistent with larger nonflow values than the nucleon participant model. The required nonflow values are essentially positive at all measured multiplicities. This means this model has a better chance of accommodating the near-side two-particle correlations observed in data.

Figure 9 (right) shows $\langle \frac{dN_{ch}}{d\eta} \rangle \delta_2$ derived using the fKLN-CGC Monte Carlo model. This model has a larger average eccentricity and smaller eccentricity fluctuations leading to the smallest relative fluctuations of the three models. The mean multiplicity scaled nonflow again is larger for 200-GeV collisions than 62.4-GeV collisions and Cu + Cu collisions seem to have the same nonflow values as Au + Au when they are compared at the same mean multiplicity. The multiplicity scaled nonflow implied by the fKLN-CGC eccentricity model increases slightly or remains flat with centrality. CGC models for the initial conditions of heavy-ion collisions have also been invoked to try to explain the near-side correlations observed in the data [37]. This analysis adds information from four-particle correlations not accessible through measurements of a two-particle correlation function. It remains to be seen if a consistent determination of two- and four-particle cumulants related to v_2, v_2 fluctuations and nonflow can be derived from a CGC model with radially boosted flux tubes. The fKLN-CGC model leaves the most room for nonflow and fluctuations from the hydrodynamic phase to contribute to event-to-event v_2 fluctuations while the the MCG-N model leaves almost no room for fluctuations beyond those from the initial eccentricity fluctuations.

C. Eccentricity scaling of v_2

We now show the ratio $\langle v_2 \rangle / \langle \varepsilon \rangle$ for the three models of eccentricity. While ideal hydrodynamic calculations suggest $v_2 \propto \varepsilon$ independent of system size, viscous effects introduce a length scale that can lead to a breakdown of $v_2 \propto \varepsilon$ for different system sizes. In the case that $v_2 \propto \varepsilon$, then $\langle v_2 \rangle / \langle \varepsilon \rangle$ in the reaction plane reference frame is given by $v_2\{4\}/\varepsilon\{4\}$ [38,39] ($\varepsilon\{4\}$ is the fourth cumulant defined in Appendix B). In the top panels of Fig. 10 we plot $v_2\{4\}/\varepsilon\{4\}$ versus mean multiplicity for Au + Au and Cu + Cu collisions at 200 and 62.4 GeV. When plotted versus mean multiplicity, all systems and energies fall on top of each other. The red line in the top panel of the figure shows a simple log-linear fitting function.
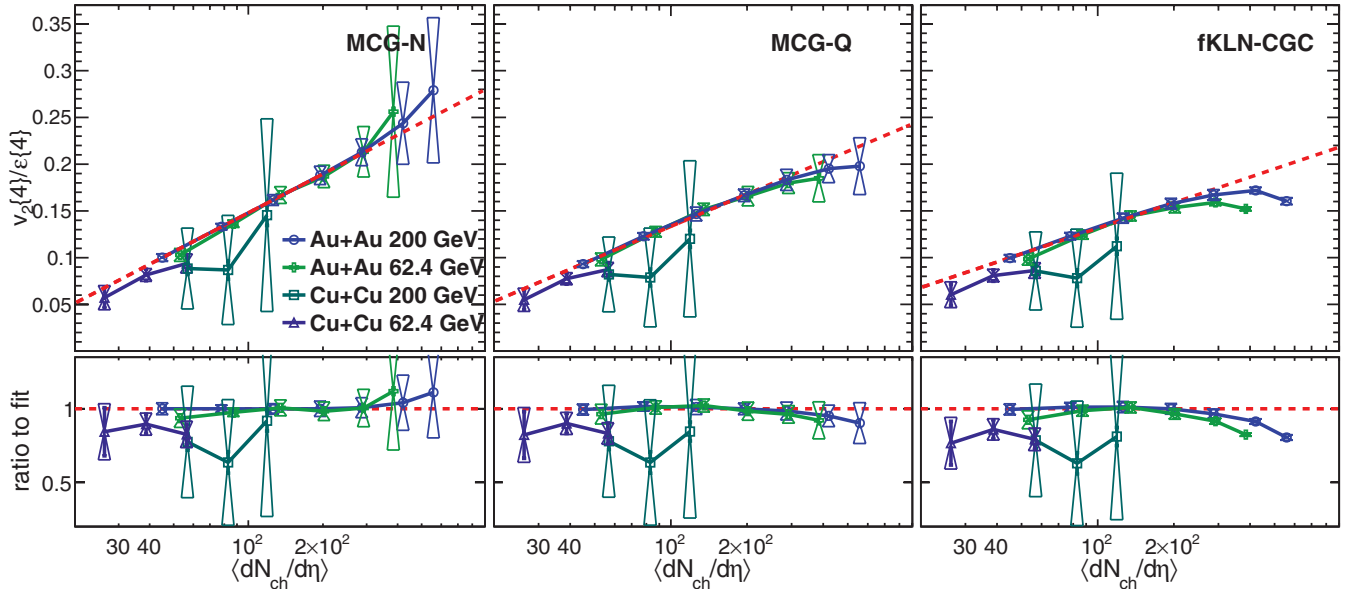
FIG. 10. (Color online) (Top panels) The eccentricity scaled v_2 for 200- and 62.4-GeV Au + Au and Cu + Cu collisions with eccentricity taken from the MCG-N (left), MCG-Q (middle), or fKLN-CGC (right) model. The statistical and systematic errors are shown as in previous figures. Statistical errors are not visible for most of the points. (Bottom panels) The ratio of the data to a log linear straight-line fit.

The bottom panels of Fig. 10 show the ratio of the data to the fit. The fKLN-CGC model displays a saturation at larger multiplicities with $v_2 \propto \varepsilon$. The Monte Carlo Glauber model with nucleon participants shows the steepest increase of v_2/ε while the constituent quark model is intermediate between the sharp rise of the nucleon participant model and the saturation of the fKLN-CGC model. The approximation that $v_2 \propto \varepsilon$ is strongly violated for the nucleon participant model with $v_2\{4\}/\varepsilon\{4\}$ increasing linearly with the log of the average multiplicity. This also implies that $v_2\{4\}/\varepsilon\{4\} = \langle v_2 \rangle / \langle \varepsilon \rangle$ may be broken since that equality holds only when $v_2 \propto \varepsilon$. The violation of $v_2 \propto \varepsilon$ also implies that if the nucleon participant model is the correct eccentricity model, then the collisions at RHIC may be far from the ideal hydrodynamic limit [40]. The centrality dependence of v_2/ε with the fKLN-CGC model and constituent quark model implies v_2 saturates or nearly saturates in central Au + Au collisions, consistent with a nearly perfect liquid behavior.

When comparing $R_{v(2-4)}$ to $R_{\varepsilon(2-4)}$, we noted that the MCG-N model leaves little room for fluctuations beyond the initial eccentricity fluctuations. Since viscous effects should contribute v_2 fluctuations [30], the large eccentricity fluctuations from the MCG-N model would imply very small viscous effects while the smaller relative eccentricity fluctuations from the fKLN-CGC model leaves room for more viscous effects. The system-size dependence of v_2/ε presented in this section, however, leads to the opposite conclusion: The increase of v_2/ε with system size when using the MCG-N model for eccentricity seems to imply the fireball is far from the ideal hydrodynamic limit, while the saturation of v_2/ε when using the fKLN-CGC model for eccentricity suggests that the fireball is close to the hydrodynamic limit [40]. It is not clear at present whether the conclusions from

event-to-event fluctuations can be reconciled with the conclusions from the centrality dependence of v_2/ε. More comprehensive theoretical studies are needed.

VI. CONCLUSIONS

We presented STAR measurements of two- and four-particle v_2 cumulants ($v_2\{2\}$ and $v_2\{4\}$) for Au + Au and Cu + Cu collisions at $\sqrt{s_{NN}} = 200$ and 62.4 GeV along with the difference $v_2\{2\}^2 - v_2\{4\}^2 \approx \delta_2 + 2\sigma_{v_2} \equiv \sigma_{tot}^2$ for charge-independent and like-sign combinations of particles. $v_2\{4\}^4$ shows negative values for the most central collisions for all the data sets, which is expected if v_2 fluctuations follow the same trend as ε_{part} fluctuations. The difference $v_2\{2\}^2 - v_2\{4\}^2$ increases with beam energy for both Cu + Cu and Au + Au collisions. For a given $\sqrt{s_{NN}}$ and mean charged-particle multiplicity, $v_2\{2\}^2 - v_2\{4\}^2$ values are the same in Cu + Cu and Au + Au collisions within errors. Although the value of v_2 fluctuations cannot be uniquely determined in this way, $v_2\{2\}$ and $v_2\{4\}$ were used to place an upper limit on the ratio σ_{v_2}/v_2. The eccentricity fluctuations from the MCG-N model are largest, rising above the upper limit from data for central Au + Au collisions, but the MCG-Q and fKLN-CGC eccentricity models fall within the presented limit. To further investigate the models we calculated the value of the nonflow δ_2 implied by the models for eccentricity fluctuations under the assumption that $\sigma_{v_2}/v_2 = \sigma_\varepsilon/\varepsilon$. The v_2 fluctuations implied by the fKLN-CGC model are larger than those from either of the Monte Carlo Glauber models. The nonflow implied by the fluctuations in the MCG models leave less room for nonflow or other sources of fluctuations. This analysis challenges theoretical models of heavy-ion collisions to describe all

features of the data including v_2, v_2 fluctuations and the various correlations data. We presented v_2/ε for the three different eccentricity models and found that the fKLN-CGC model for eccentricity leads to a saturation of v_2/ε for Au + Au collisions with $\langle \frac{dN_{ch}}{d\eta} \rangle > 300$ while v_2/ε is rising at all centralities when the MCG-N model is used for ε. The MCG-Q model is intermediate between the two. Assuming fKLN-CGC to describe the initial state eccentricity, the saturation of v_2/ε provides support for a nearly perfect hydrodynamic behavior for heavy-ion collisions at RHIC.

APPENDIX A: *Q*-CUMULANTS VERSUS FITTING *q*-DISTRIBUTIONS

The fitting of the reduced flow vector distribution is described in more detail in Ref. [19]. The fit parameters described in that reference can be transformed to $v_2\{2, \text{qfit}\}^2 \equiv v_2\{\text{qfit}\}^2 + \sigma_{\text{tot}}^2$ and $v_2\{4, \text{qfit}\}^2 = v_2\{\text{qfit}\}^2$, where $v_2\{2, \text{qfit}\}$ and $v_2\{4, \text{qfit}\}$ are the two- and four-particle cumulants determined from the q-distribution which can be compared to other determinations of $v_2\{2\}$ and $v_2\{4\}$. In Fig. 11 (top) we show the ratio of $v_2\{2\}$ determined from the q-distribution analysis and the Q-cumulants analysis.

Deviations between the q-distribution and Q-cumulants results can be seen when the multiplicity of the event is smaller, with the q-distribution results being smaller than the Q-cumulants results. These deviations can be traced to the breakdown of the large N approximation required when fitting the q-distribution. An attempt is made to correct for this breakdown which brings the results closer together but the deviations are still significant for multiplicities below 150. The correction is carried out by adjusting the q-distribution data before it is fit. The correction is derived by taking the ratio of the expected and observed q-distribution from simulated data. Although the correction extends the apparent validity of the q-distribution analysis to lower multiplicities, we find that the q-distribution analysis is less reliable than the Q-cumulants analysis.

Figure 11 (bottom) shows the ratio of the quantity $v_2\{2\}^2 - v_2\{4\}^2$ from the q-distribution fits over the same from the Q-cumulants analysis. Data are from 200-GeV Au + Au and Cu + Cu collisions. The two methods produce significantly
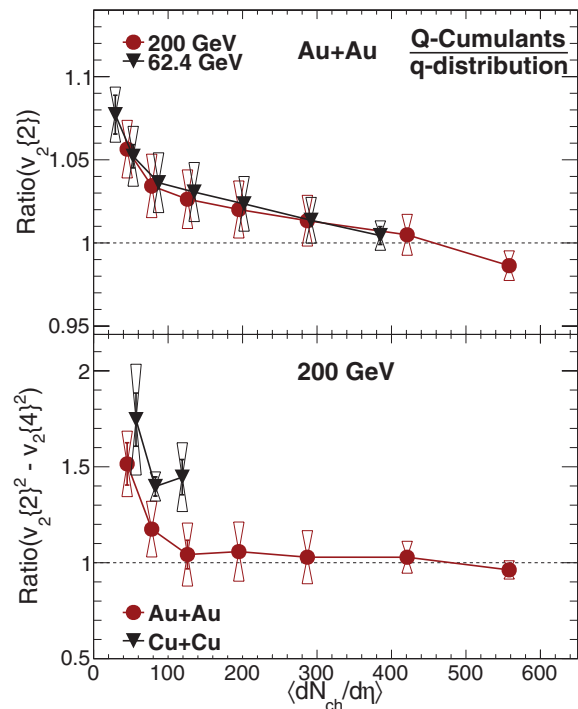

FIG. 11. (Color online) (Top panel) The ratio of the two-particle cumulant $v_2\{2\}$ for Au + Au collisions at 200 and 62.4 GeV evaluated using the q-distribution method and the Q-cumulants method. Both results are calculated for combinations of particles independent of their charge (CI). (Bottom panel) The ratio of the q-distribution and the Q-cumulants method results for $v_2\{2\}^2 - v_2\{4\}^2$ (CI) for 200-GeV Au + Au and Cu + Cu collisions. In both panels, systematic errors are shown as triangles above and below the data points and statistical errors are shown as thick lines with caps.

different results for $v_2\{2\}^2 - v_2\{4\}^2$ with the difference most pronounced in Cu + Cu and peripheral Au + Au collisions. The q-distribution gives smaller values. This is related to the large N approximation required in the fitting procedure for the q-distribution. When multiplicity is low, the tails of the q-distribution cannot be populated. We find that this leads to a narrowing of the observed distribution relative to the fit function and the width of the distribution determines $v_2\{2\}^2 - v_2\{4\}^2$. The q-distribution fits therefore underestimate $v_2\{2\}^2 - v_2\{4\}^2$, so we use the results from the Q-cumulants calculation in this paper.

APPENDIX B: THREE ECCENTRICITY MODELS

We use three Monte Carlo models to study eccentricity and eccentricity fluctuations. The first two are Glauber models which treat nucleons either as participants or constituent quarks within the nucleons as participants (MCG-N and MCG-Q, respectively). The third model is the factorized Kharzeev, Levin, and Nardi color glass condensate model (fKLN-CGC) [13]. The input parameters used for the Woods-Saxon distribution of nucleons are in Table II. The Au nuclei have been assumed spherical for the eccentricity calculations. A 0.4-fm exclusion radius is used in the calculations so

TABLE II. Input parameters for Woods-Saxon distribution in Monte Carlo models.

Parameter/system	^{197}Au + ^{197}Au	^{63}Cu + ^{63}Cu
R	6.38 ± 0.06 fm	4.218 ± 0.014 fm
a	0.535 ± 0.027 fm	0.596 ± 0.005 fm

nucleons do not overlap in coordinate space. The MCG-N model is described elsewhere [7,41] and is used to calculate the N_{part} and N_{bin} values in Table III. For the MCG-Q model, we, first, distribute nucleons inside a nucleus according to a Woods-Saxon distribution with parameters taken from Ref. [42] and then distribute three constituent quarks inside each nucleon according to another Woods-Saxon distribution where the radius of the nucleon is taken to be 0.63 fm and the surface width is 0.08 fm. The results were not very sensitive to variations of these parameters within a reasonable range. One might consider a Gaussian for the quarks instead of a Woods-

TABLE III. The $\langle dN_{ch}/d\eta \rangle$ [45], N_{part} and N_{bin} values corresponding to the centrality intervals used in this paper.

Centrality (%)	$\langle dN_{ch}/d\eta \rangle$	N_{part}	N_{bin}
	Au + Au 200 GeV		
70–80%	22 ± 2	13.46 ± 0.50	12.45 ± 0.69
60–70%	45 ± 3	26.62 ± 0.95	29.33 ± 1.75
50–60%	78 ± 6	47.06 ± 1.21	62.1 ± 2.1
40–50%	126 ± 9	75.58 ± 1.56	121.8 ± 4.2
30–40%	195 ± 14	114.81 ± 1.73	218.9 ± 6.1
20–30%	287 ± 20	166.85 ± 1.33	371.3 ± 6.2
10–20%	421 ± 30	234.49 ± 0.84	599.6 ± 4.5
5–10%	558 ± 40	299.47 ± 0.75	845.6 ± 3.2
0–5%	691 ± 49	349.09 ± 0.30	1059 ± 3
	Au + Au 62.4 GeV		
70–80%	13.9 ± 1.1	13.18 ± 0.71	11.6 ± 0.87
60–70%	29.1 ± 2.2	25.56 ± 1.11	26.69 ± 1.87
50–60%	53.1 ± 4.2	44.97 ± 1.27	55.9 ± 2.9
40–50%	87.2 ± 7.1	72.70 ± 1.25	107.4 ± 3.8
30–40%	135 ± 11	110.53 ± 1.05	190.5 ± 4.5
20–30%	202 ± 17	161.08 ± 0.97	319.4 ± 4.8
10–20%	292 ± 25	228.51 ± 0.52	514.6 ± 3.4
5–10%	385 ± 33	293.39 ± 0.96	721.7 ± 3.9
0–5%	472 ± 41	343.82 ± 0.44	900.75 ± 1.85
	Cu + Cu 200 GeV		
50–60%	25.3 ± 1.6	16.41 ± 0.24	15.71 ± 0.31
40–50%	38.7 ± 2.5	25.14 ± 0.16	27.42 ± 0.22
30–40%	56.9 ± 3.7	37.35 ± 0.47	46.87 ± 1.00
20–30%	82.9 ± 5.4	53.07 ± 0.29	75.46 ± 0.42
10–20%	119 ± 7.7	73.61 ± 0.12	119.65 ± 0.15
0–10%	170 ± 11	98.08 ± 0.11	182.7 ± 0.30
	Cu + Cu 62.4 GeV		
50–60%	17.4 ± 1.1	15.36 ± 0.05	13.91 ± 0.01
40–50%	26.3 ± 1.7	23.92 ± 0.05	25.56 ± 0.06
30–40%	38.7 ± 2.5	35.62 ± 0.05	41.09 ± 0.12
20–30%	56.4 ± 3.7	50.76 ± 0.12	65.86 ± 0.30
10–20%	81.2 ± 5.3	70.67 ± 0.50	103.15 ± 0.95
0–10%	117 ± 7.7	94.98 ± 0.25	155.65 ± 0.75

Saxon distribution. The Woods-Saxon distribution gives a more flat-topped distribution but the calculated eccentricity and eccentricity fluctuations are not highly sensitive to the exact distribution. The main feature of the MCG-Q model is that the potential number of participants increases by a factor of 3 and there are large correlations between participants because the quarks are confined within the nucleons.

The Woods-Saxon parameters from Ref. [42] are based on measurements of electron scattering which are sensitive only to protons. If the Au nucleus has a neutron skin, then the hadronic radius may be larger than that quoted in Ref. [42]. We estimated the systematic errors by varying the Woods-Saxon parameters within the range allowed by electron-scattering data. Although unmeasured, theoretical guidance suggests the neutron skin may add 0.2 fm to the radius of heavy nuclei [43]. To account for a possible neutron skin, we increased the radius of the Au nucleus to 6.7 fm. We find that our results only weakly depend on the radius and depend mostly on the diffuseness parameter "a." The effect of a neutron skin is, therefore, well within our quoted systematic errors and will not affect our conclusions unless the skin significantly changes the diffuseness at the edge of the nucleus.

The fKLN-CGC model provides multiplicity and eccentricity. Our MCG calculations use a two-component model and a negative binomial distribution to estimate the event multiplicity for each simulated event. The first parameter of the binomial distribution is generated for each event using

$$\bar{n} = f(\sqrt{s_{NN}})((1 - x_{hard}) + 2x_{hard}N_{bin}/N_{part}), \quad \text{(B1)}$$

where $f(\sqrt{s_{NN}}) = 0.5933 \ln(\sqrt{s_{NN}}/\text{GeV}/c^2) - 0.4153$, N_{bin} is the number of nucleon-nucleon collisions, N_{part} is the
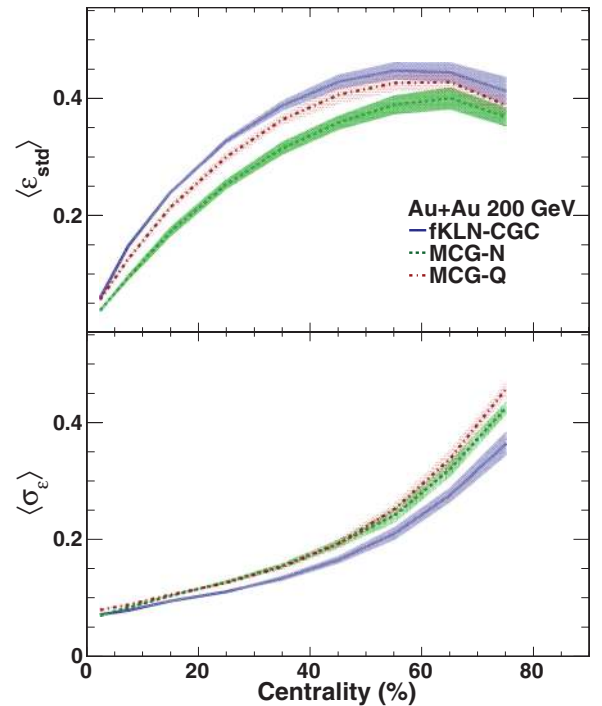

FIG. 12. (Color online) ε_{std} (top) and σ_ε (bottom) vs. centrality for Au + Au 200 GeV among the Monte Carlo Glauber-nucleon participants, Monte Carlo Glauber-quark constituents, and color glass condensate models. The shaded regions show the systematic errors.

number of participating nucleons, and x_{hard} is the fraction of the multiplicity proportional to N_{bin}. Multiplicity then is generated by sampling a negative binomial distribution with parameters $\bar{n}$ and width $k = 2.1$ for each participant. This parametrization provides a good description of multiplicity measurements in heavy-ion collisions from $\sqrt{s_{NN}} = 20$ to 200 GeV [44] and for all centralities. For the MCG-Q model, while the eccentricity is defined by the locations of constituent quarks participating in the collisions, the multiplicity is defined by the nucleon N_{part} and N_{bin}. We define the centrality of the models according to this multiplicity so the data and model are treated equivalently. In this way, our eccentricity fluctuations also contain the impact parameter and N_{part} fluctuations that are intrinsic to our experimental determination of a given centrality interval. The uncertainties on the models were estimated by varying the Woods-Saxon parameters within the range of the errors quoted in Ref. [42]. We also varied the parameters for the multiplicity but the results were not very sensitive to those.

Several different variables related to the eccentricity have been calculated from the three models. This includes the eccentricity relative to the reaction plane ($\varepsilon_{std} = \frac{\langle y-x\rangle}{\langle y+x\rangle}$), the eccentricity relative to the participant plane (ε_{part}), and the two- and four-particle cumulants of ε_{part} [38,39],

$$\varepsilon\{2\} = \sqrt{\langle \varepsilon_{part}^2\rangle}, \tag{B2}$$

$$\varepsilon\{4\} = \left(2\langle \varepsilon_{part}^2\rangle^2 - \langle \varepsilon_{part}^4\rangle\right)^{1/4}, \tag{B3}$$

where ε_{std} for 200 GeV Au + Au collisions is shown in Fig. 12 (top). ε_{std} is largest for the fKLN-CGC model and smallest in the MCG-N model. The MCG-Q model is intermediate between the two. The relevant quantities have been tabulated online [29].

Figure 12 (bottom) shows the fluctuations of ε_{std} for the three models for 200-GeV Au + Au collisions. The fluctuations in the two Glauber models are larger than those for the fKLN-CGC model. One might expect the MCG-Q model to have smaller fluctuations than the MCG-N model since there are 3 times as many possible participants. This is counterbalanced, however, by two effects: (1) the three constituent quarks are confined inside nucleons, thus inducing correlations that partially offset the effect of more participants, and (2) the mean value of the eccentricity is larger in the MCG-Q model. These effects lead to the result that the width of the eccentricity distribution in the MCG-Q model and the MCG-N model are similar. On the other hand, since the MCG-Q model gives a larger average eccentricity, when considering $\sigma_\varepsilon/\varepsilon$, the MCG-Q model is intermediate between the fKLN-CGC and the MCG-N models as one might naively expect.

The trends for Cu + Cu collisions remain the same as for Au + Au collisions with the fKLN-CGC model having the
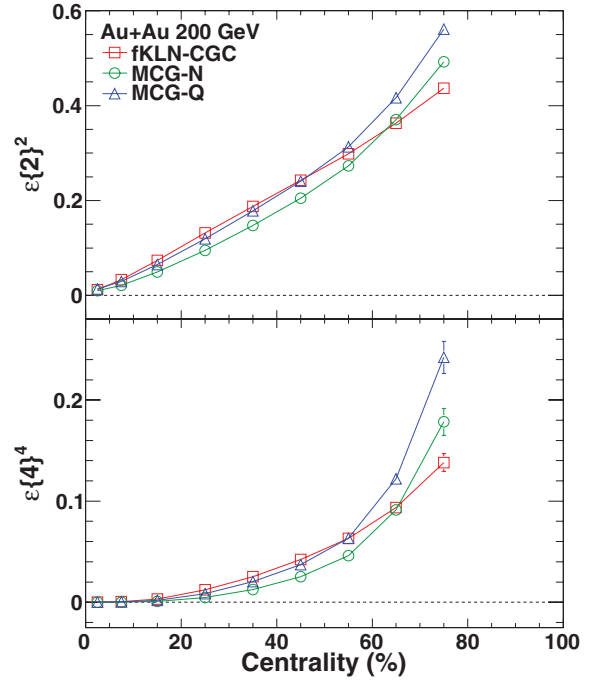

FIG. 13. (Color online) $\varepsilon\{2\}^2$ and $\varepsilon\{4\}^4$ vs. centrality for Monte Carlo Glauber models with nucleon or constituent quark pariticipants and for a color glass condensate model.

largest eccentricity and smallest fluctuations and the MCG-Q model intermediate between the MCG-N and fKLN-CGC models. None of the models showed a significant difference between $\sqrt{s_{NN}} = 62.4$ and 200 GeV, so we show only the 200-GeV results here.

Figure 13 shows $\varepsilon\{2\}^2$ (top) and $\varepsilon\{4\}^4$ (bottom) for Au + Au 200 GeV for the three models. $\varepsilon\{2\}^2$ shows positive values throughout the range and decreases with increasing centrality. The MCG-N model shows smaller values than the other two models for central and mid-central collisions but cross fKLN-CGC for the most peripheral collisions. MCG-Q and fKLN-CGC models show the same values for $\varepsilon\{2\}^2$ for central and midcentral collisions but MCG-Q shows the highest values in all the three models for the most peripheral collisions. $\varepsilon\{4\}^4$ shows similar behavior as $\varepsilon\{2\}^2$ but it becomes negative for the most central collisions in all the models like $v_2\{4\}^4$ for the most central collisions in the data. This behavior is the same for Cu + Cu collisions and different energies. In the models, this negative value can be traced to N_{part} fluctuations present when using multiplicity to select centrality bins. If N_{part} is used to define the centrality in the models, then $\varepsilon\{4\}^4$ remains positive, even for central collisions.

[1] J.-Y. Ollitrault, Phys. Rev. D **46**, 229 (1992); H. Sorge, Phys. Rev. Lett. **82**, 2048 (1999).

[2] K. H. Ackermann *et al.* (The STAR Collaboration), Phys. Rev. Lett. **86**, 402 (2001).

[3] B. B. Back *et al.* (The PHOBOS Collaboration), Phys. Rev. Lett. **89**, 222301 (2002); K. Adcox *et al.* (The PHENIX Collaboration), *ibid.* **89**, 212301 (2002).

[4] P. F. Kolb, J. Sollfrank, and U. W. Heinz, Phys. Rev. C **62**, 054909 (2000).

[5] M. Harrison, T. Ludlam, and S. Ozaki, Nucl. Instrum. Methods A **499**, 235 (2003).

[6] S. Voloshin and Y. Zhang, Z. Phys. C **70**, 665 (1996).

[7] B. Alver *et al.*, Phys. Rev. C **77**, 014906 (2008).

[8] K. H. Ackermann *et al.* (The STAR Collaboration), Phys. Rev. Lett. **86**, 402 (2001); C. Adler (The STAR Collaboration), *ibid.* **87**, 182301 (2001); **89**, 132301 (2002); J. Adams *et al.* (The STAR Collaboration), *ibid.* **92**, 052302 (2004); Phys. Rev. C **72**, 014904 (2005); Phys. Rev. Lett. **95**, 122301 (2005); K. Adcox *et al.* (The PHENIX Collaboration), Nucl. Phys. A **757**, 184 (2005); J. Adams *et al.* (The STAR Collaboration), *ibid.* **757**, 102 (2005); B. Alver *et al.* (The PHOBOS Collaboration), Phys. Rev. Lett. **98**, 242302 (2007); B. B. Back *et al.* (The PHOBOS Collaboration), Phys. Rev. C **72**, 051901(R) (2005); Phys. Rev. Lett. **94**, 122303 (2005); B. I. Abelev *et al.* (The STAR Collaboration), Phys. Rev. C **75**, 054906 (2007); **77**, 054901 (2008); **81**, 044902 (2010).

[9] P. Danielewicz and M. Gyulassy, Phys. Rev. D **31**, 53 (1985).

[10] P. K. Kovtun, D. T. Son, and A. O. Starinets, Phys. Rev. Lett. **94**, 111601 (2005).

[11] P. Huovinen, P. F. Kolb, U. W. Heinz, P. V. Ruuskanen, and S. A. Voloshin, Phys. Lett. B **503**, 58 (2001); D. Teaney, Phys. Rev. C **68**, 034913 (2003); K. Dusling and D. Teaney, *ibid.* **77**, 034905 (2008); U. Heinz *et al.*, arXiv:1108.5323v1 [nucl-th].

[12] T. Hirano, U. W. Heinz, D. Kharzeev, R. Lacey, and Y. Nara, Phys. Lett. B **636**, 299 (2006); T. Lappi and R. Venugopalan, Phys. Rev. C **74**, 054905 (2006).

[13] A. Adil, H. J. Drescher, A. Dumitru, A. Hayashigaki, and Y. Nara, Phys. Rev. C **74**, 044905 (2006); H. J. Drescher and Y. Nara, *ibid.* **76**, 041903 (2007).

[14] A. M. Poskanzer and S. A. Voloshin, Phys. Rev. C **58**, 1671 (1998).

[15] M. Miller and R. Snellings, arXiv:nucl-ex/0312008v2.

[16] J. Y. Ollitrault, A. M. Poskanzer, and S. A. Voloshin, Phys. Rev. C **80**, 014904 (2009).

[17] S. A. Voloshin, A. M. Poskanzer, A. Tang, and G. Wang, Phys. Lett. B **659**, 537 (2008).

[18] J. Adams *et al.* (The STAR Collaboration), Phys. Rev. C **72**, 014904 (2005).

[19] P. Sorensen (The STAR Collaboration), J. Phys. G **35**, 104102 (2008).

[20] J. Adams *et al.* (The STAR Collaboration), Phys. Rev. C **73**, 064907 (2006).

[21] G. Agakishiev *et al.*, arXiv:1109.4380v2 [nucl-ex].

[22] K. H. Ackermann *et al.* (The STAR Collaboration), Nucl. Instrum. Meth. A **499**, 624 (2003).

[23] K. H. Ackermann *et al.* (The STAR Collaboration), Nucl. Phys. A **661**, 681 (1999).

[24] J. Adams *et al.* (The STAR Collaboration), Phys. Rev. Lett. **92**, 052302 (2004).

[25] J. Adams *et al.* (The STAR Collaboration), Phys. Rev. C **73**, 034906 (2006).

[26] A. Bilandzic, R. Snellings, and S. Voloshin, Phys. Rev. C **83**, 044913 (2011).

[27] K. Aamodt *et al.* (The ALICE Collaboration), Phys. Rev. Lett. **105**, 252302 (2010).

[28] P. Abreu *et al.* (The DELPHI Collaboration), Phys. Lett. B **407**, 174 (1997).

[29] Link to tables of numbers: [http://www.star.bnl.gov/protected/bulkcorr/nav/paper_preview/preview.html].

[30] S. Vogel, G. Torrieri, and M. Bleicher, Phys. Rev. C **82**, 024908 (2010).

[31] Z. Qiu and U. Heinz, Phys. Rev. C **84**, 024911 (2011).

[32] P. Filip, R. Lednicky, H. Masui, and N. Xu, Phys. Rev. C **80**, 054903 (2009).

[33] G. S. F. Stephans, J. Phys. G **32**, S447 (2006); P. Sorensen (The STAR Collaboration), PoS(CPOD2006)020; T. Satogata *et al.*, PoS(CPOD07)051; M. M. Aggarwal *et al.* (The STAR Collaboration), arXiv:1007.2613v1 [nucl-ex].

[34] B. Alver *et al.* (The PHOBOS Collaboration), Phys. Rev. C **81**, 034915 (2010).

[35] P. Bozek, W. Broniowski, and J. Moreira, Phys. Rev. C **83**, 034911 (2011).

[36] J. Adams *et al.* (The STAR Collaboration), Phys. Rev. C **75**, 034901 (2007).

[37] A. Dumitru, F. Gelis, L. McLerran, and R. Venugopalan, Nucl. Phys. A **810**, 91 (2008).

[38] S. A. Voloshin, arXiv:nucl-th/0606022v2.

[39] R. S. Bhalerao and J. Y. Ollitrault, Phys. Lett. B **641**, 260 (2006).

[40] H.-J. Drescher, A. Dumitru, C. Gombeaud, and J.-Y. Ollitrault, Phys. Rev. C **76**, 024905 (2007).

[41] M. L. Miller, K. Reygers, S. J. Sanders, and P. Steinberg, Annu. Rev. Nucl. Part. Sci. **57**, 205 (2007).

[42] H. De Vries, C. W. De Jager, and C. De Vries, At. Data Nucl. Data Tabl. **36**, 495 (1987).

[43] W. D. Myers and W. J. Swiatecki, Nucl. Phys. A **336**, 2 (1980); L. W. Chen, C. M. Ko, and B. A. Li, Phys. Rev. C **72**, 064309 (2005).

[44] B. B. Back *et al.* (The PHOBOS Collaboration), Phys. Rev. C **70**, 021902 (2004).

[45] B. I. Abelev *et al.* (STAR Collaboration), Phys. Rev. C **79**, 034909 (2009).